Electronic Supplementary Information (ESI) for

Title: Proton-Electron-Coupled MoS_2 Synaptic Transistors with a Natural Renewable Biopolymer Neurotransmitter for Brain-Inspired Neuromorphic Learning†

Wennan Hu, Jie Jiang*, Dingdong Xie, Biao Liu, Junliang Yang and Jun He*

Hunan Key Laboratory of Super Microstructure and Ultrafast Process, School of Physics and Electronics, Central South University, Changsha, Hunan 410083, China

* Corresponding author(s): jiangjie@csu.edu.cn; junhe@csu.edu.cn

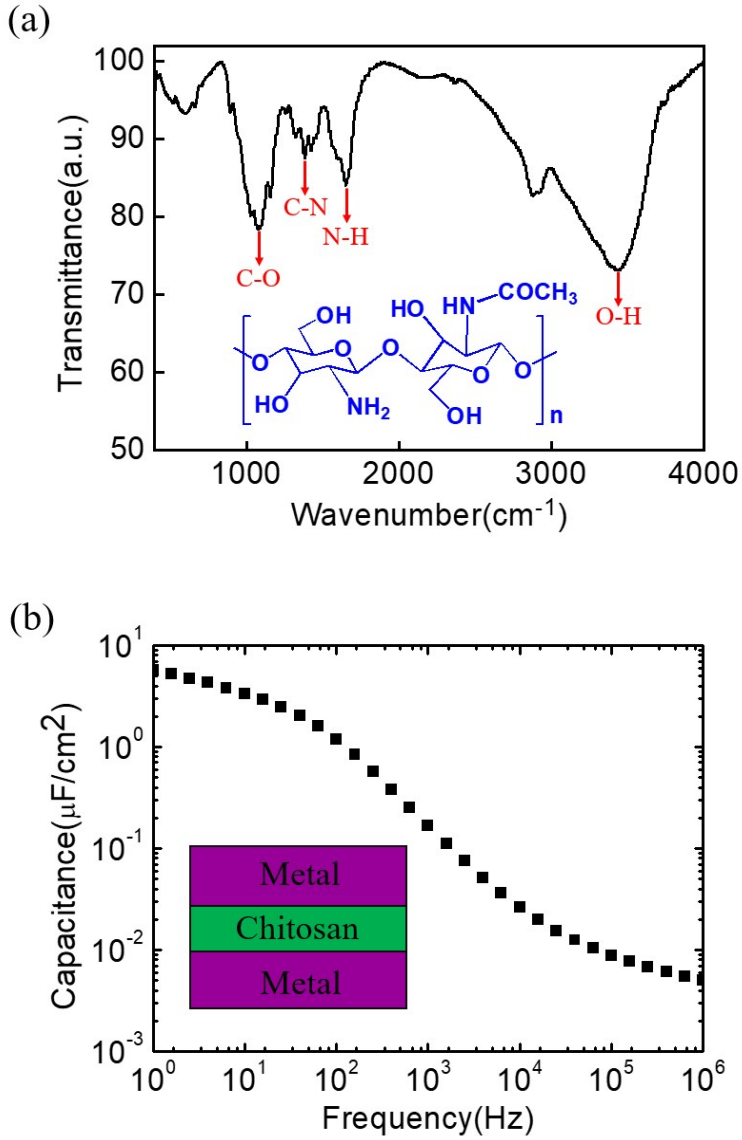

Fig. S1 (a) The FTIR spectra of chitosan film. Inset: the molecular structure of chitosan. (b) Frequency-dependent capacitance curve of the chitosan film with a vertical metal/chitosan/metal sandwich structure.

The broad band at 3438 cm^{-1} is ascribed to the O-H stretching, while the bending vibration of C-O locates at 1078 cm^{-1}.[1] Besides, the amide (C-N) band appears at around 1382 cm^{-1} and the remaining characteristic band at 1654 cm^{-1} corresponds to the N-H bending of $-NH_2$.[2]

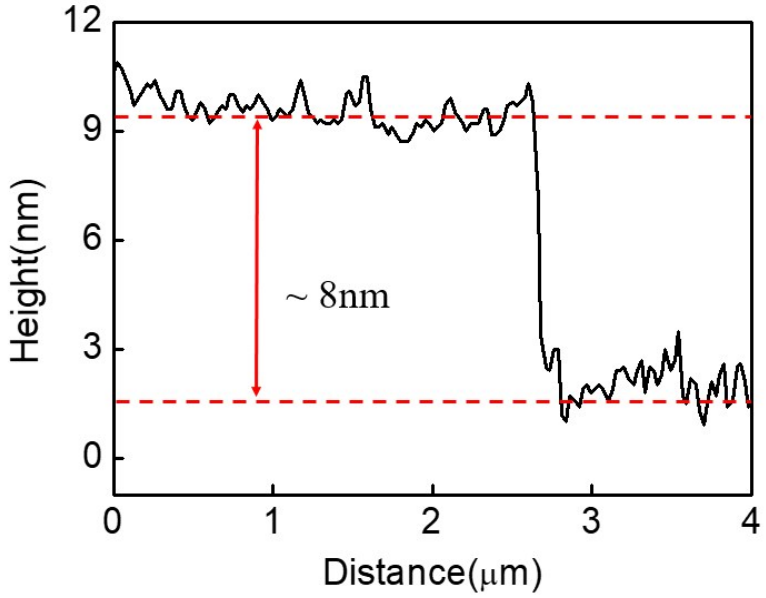

Fig. S2 The thickness of as-fabricated MoS_2 flake measured by AFM.

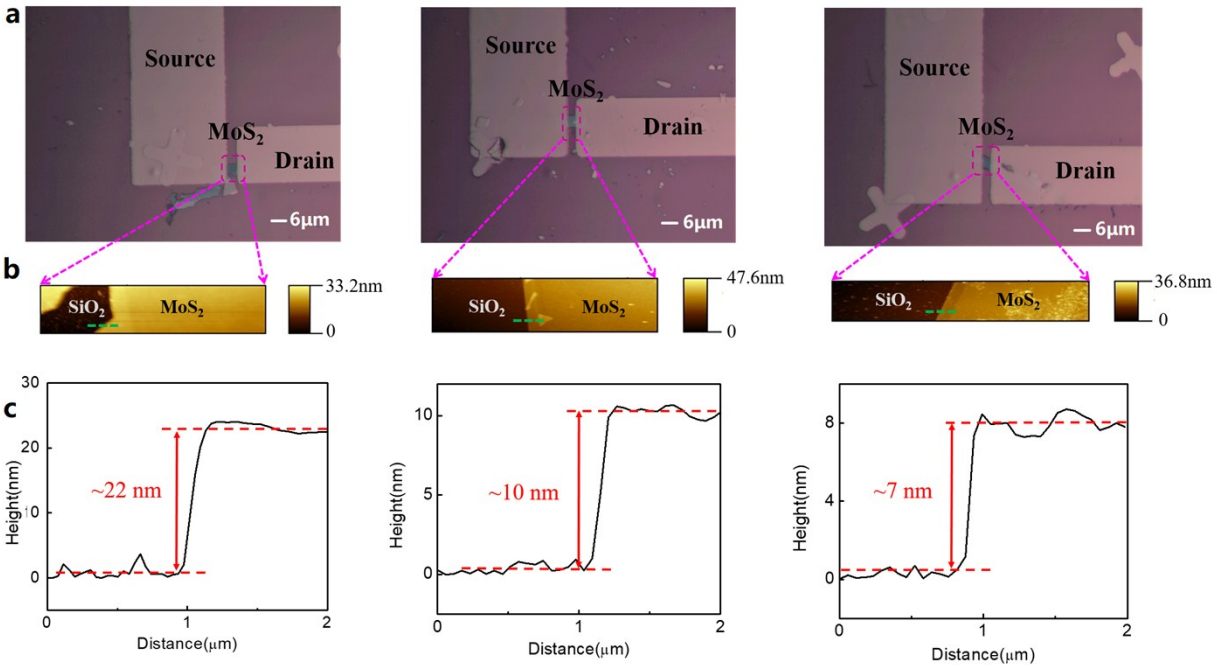

Fig. S3 (a) Optical top-view images of the MoS_2 FET. Scale bar of inset: 6 μm. (b) The morphology of the MoS_2 films characterized by AFM. (c) The different thickness of as-fabricated MoS_2 flakes extracted from AFM measurements.

We have fabricated three different MoS_2 transistors and the optical top-view images of the devices are shown in Figure S3a above, where two metal electrodes are bridged by a MoS_2 flake and the channel length is the same as 6 μm. Moreover, the AFM surface morphology images of MoS_2 flakes are measured as shown in Figure S3b above, and at the same time the thickness of the MoS_2 flakes can also be obtained by AFM, as shown in Figure S3c above, which is 22 nm, 10nm and 7nm, respectively.

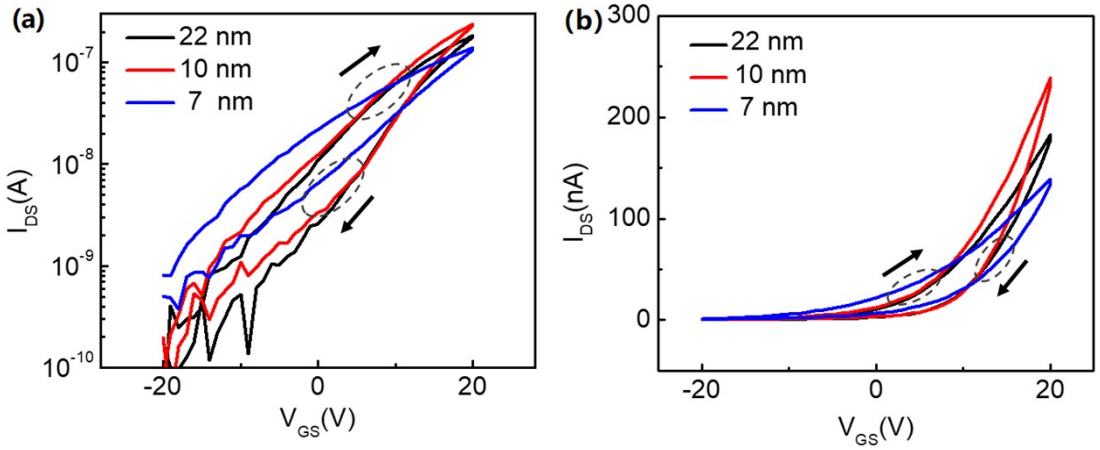

Fig. S4 (a) The logarithmic transfer curves for the back-gated MoS_2 FET with different MoS_2 thickness. (b) The linear transfer curves.

To further investigate the influence of the MoS_2 thickness on the transistor performance, the transfer curves for the back-gated MoS_2 FETs are shown in Figure S4a (logarithmic) and S4b (linear) above with a fixed V_{DS} of 0.1 V. As we see, the devices with a MoS_2 thickness of 7 nm and 10 nm exhibit the smallest and largest on-state current respectively, while 22 nm thick device is in the middle. Besides, field-effect mobility values (μ) were also found to depend strongly on the MoS_2 flake thickness, where μ=10.3cm^2/Vs (7nm), 21cm^2/Vs (10nm) and 15.3cm^2/Vs (22nm), respectively. Therefore, in our experiment, 10 nm thick MoS_2 FET relatively exhibits the best device performance with a maximum mobility value and on-state current. Our such results are very consistent with the previous reports,[3] in which Das *et al* have demonstrated that the performance of devices with a MoS_2 layer thickness in the range of 0~12 nm is getting better and then it would go down.

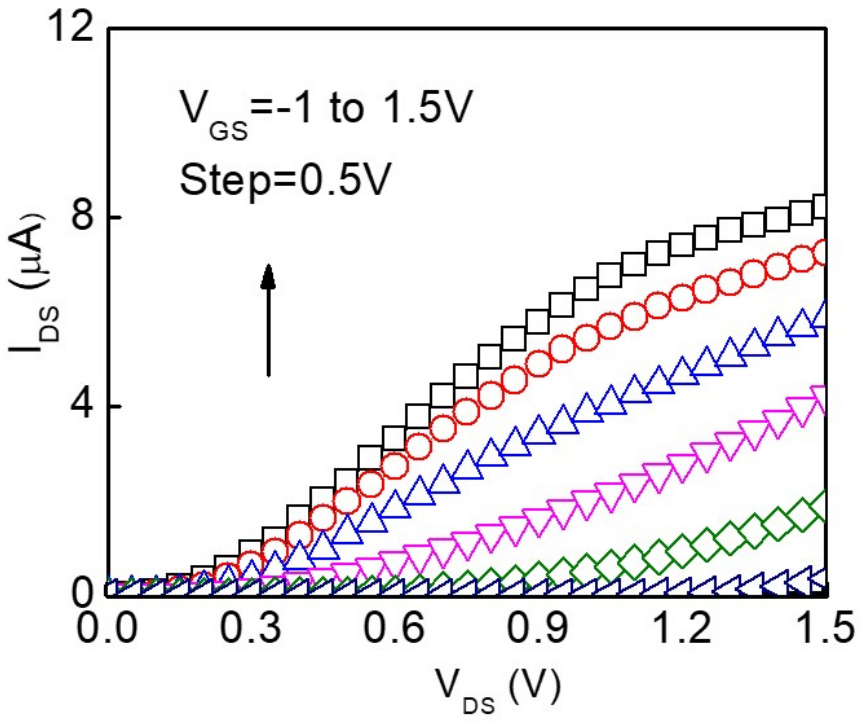

Fig. S5 The output characteristic of the MoS_2 transistor.

It exhibits a clear linear relationship at low V_{DS} region and a good pinch-off behavior at high V_{DS} region, thereby verifying the formation of typical n-channel field-effect operation mode.

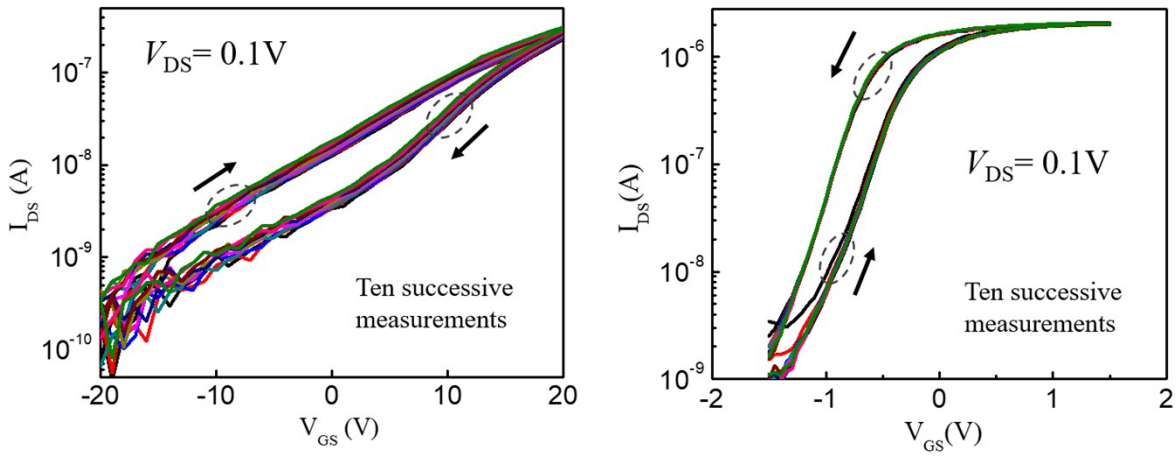

Fig. S6 (a) Original transfer curve with ten successive measurements for the back-gated MoS_2 FET before chitosan coating. (b) Transfer curve with ten successive measurements for the side-gated MoS_2 FET after chitosan coating.

We tested the original transfer curve for the back-gated MoS_2 FET before chitosan coating process, as shown in Fig. S6a above. We can see that the back-gated device exhibits a large operation voltage of ~20V with a clockwise hysteresis window. However, after chitosan coating, the side-gated EDL MoS_2 FET shows a low working voltage of ~1.5V with a different hysteresis direction: anticlockwise, as shown in Fig. S6b above. According to the FET theory, the clockwise hysteresis means charge trapping mechanism, while anticlockwise hysteresis means mobile ion mechanism.[4,5] Therefore, the present side-gated EDL MoS_2 FET is mobile proton modulation mechanism rather than charge trapping mechanism. Our presented MoS_2 synaptic device is only a proof-of-principle study to demonstrate its technological feasibility. In our study, the MoS_2 transistor exhibits a reasonable stability and reproducibility after ten successive measurements, as shown in Figure S6 above.

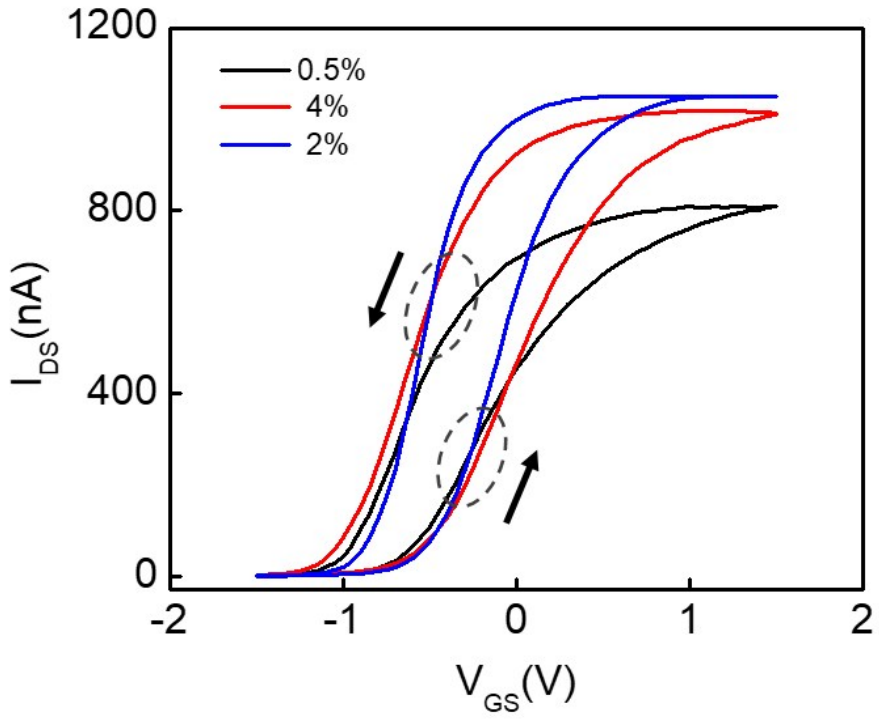

Fig. S7 Transfer curves for different chitosan composition (0.5 wt%, 2 wt% and 4 wt% in acetic acid).

In our experiment, the acetic acid is used as solvent to prepare the chitosan solution. When chitosan molecular reacts with water, positively protonated amino groups (NH_3^+) and OH^- anions will be generated.[6] Due to the existence of acetic acid, this reversible reaction would prefer to move along the forward direction, and many protonated amino groups appear finally. Under an external electric field, a portion of protonated amino groups will become deprotonated, as shown in Figure 1c in our main manuscript, resulting in a sequence of protons hopping from one oxygen atom to another.[7] Based on the above theory, we prepared three different chitosan solutions respectively with the acetic acid concentrations of 0.5%, 2% and 4%, to study the effect of chitosan composition on the device performance. Herein, in order to ensure the reliability of test results, the well-prepared three kinds of chitosan solution were respectively drop-casted

onto the top of the same MoS_2 FET. (After a testing, we will use the corresponding acetic acid solvent to dissolve the chitosan electrolyte and wash it repeatedly with DI water and then drop-cast another solution and conduct the next experiment.) Transfer curves for three chitosan composition are shown in Figure S7 above. We can observe that on-state current is obviously smaller for 0.5% acetic acid than that of 2% and 4%. That is because relatively less acetic acid produces less protonated amino groups and image charges induced by electrostatic coupling. However, it is interesting to find that on-state current for 2% acetic acid is slightly larger than 4%. We think it is possible that some of the protons for 4% acetic acid may happen the electrochemical proton-doping process, thus lowering the on-state current. Moreover, for the forward sweeping process, the field-effect mobility (μ_{FE}) and subthreshold swing (SS) can also be calculated respectively, where the μ_{FE}=18.6 cm^2/Vs (0.5%), 29.8 cm^2/Vs (2%), 23.8 cm^2/Vs (4%) and SS=0.37V/dec (0.5%), 0.35V/dec (2%), 0.41V/dec (4%). Consequently, the optimized device with 2% acetic acid shows the best performance with a largest on-state current, a largest field-effect mobility, and a smallest subthreshold swing. Therefore, based on the above considerations, we choose 2% acetic acid solvent in our experiment.

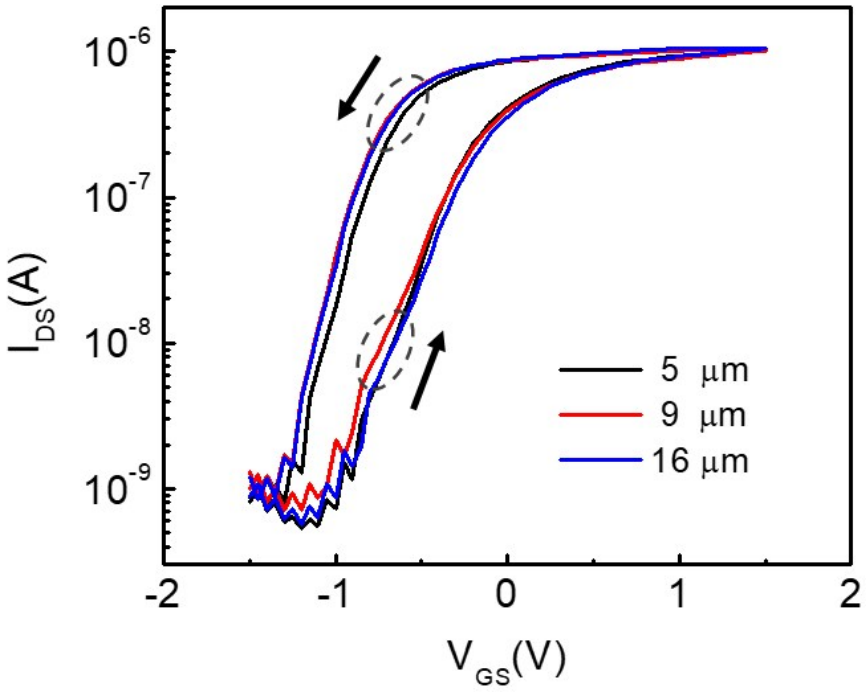

Fig. S8 Transfer curves for different chitosan thickness.

In order to study the effect of chitosan thickness on device performance, chitosan solution (2% acetic acid) with three different thicknesses was respectively drop-casted onto the top of the same MoS_2 FET. Figure S8 above shows the transfer characteristics of the device for three different chitosan thicknesses (5μm, 9μm and 16μm, measured by Step Profiler). It is clear that they are almost unchanged between each other. Therefore, we can conclude that, with the same concentration of acetic acid, the thickness of chitosan has little effect on device performance.

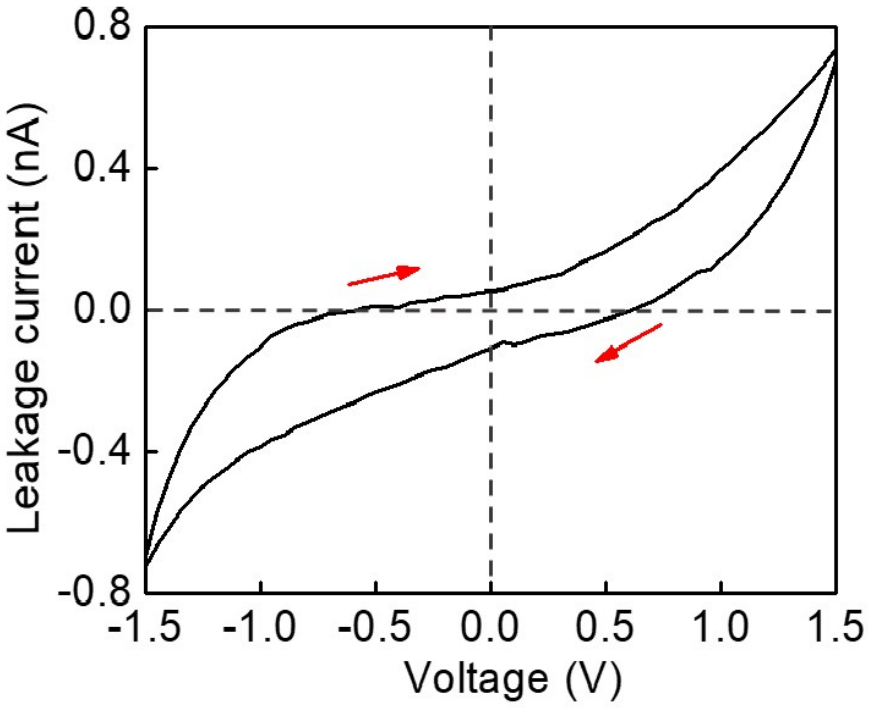

Fig. S9 The leakage current of the device between the forward and reverse V_{GS} scanning.

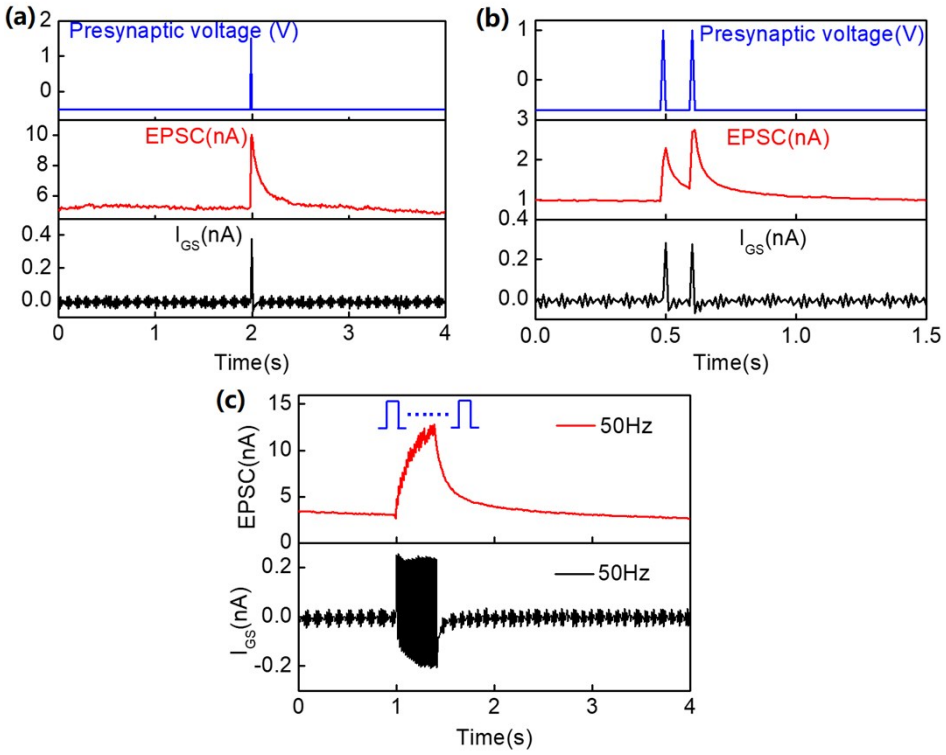

Fig. S10 The EPSCs and gate current triggered by (a) a presynaptic spike (1.5V, 10ms) (b) a pair of presynaptic spike (1V, 10ms) with an inter-spike interval (100ms) (c) a pulse train at f = 50 Hz where the pulse width and number are respectively fixed to 10 ms and 20.

We have plotted the corresponding drain and gate current curves, as shown in Figure S10 above. We can readily calculate that, for a single EPSC response (Figure S10a above), about 3.8% of the drain current is from gate displacement current and 96.2% is from the source. For the PPF behavior (Figure S10b above), about 9.6% of the drain current is from gate displacement current and 90.4% is from the source. And for the continuous EPSC responses (Figure S10c above), the values of that are 1.9% and 98.1%, respectively. Therefore, we can conclude that the gate current accounts for a small proportion, while the drain current mostly comes from the source. In addition, we can also find that there is no ion relaxation phenomenon in all of gate displacement currents after removing the gate bias, indicating that the synaptic behaviors of the device are attributed to the drain current rather than the gate displacement currents.

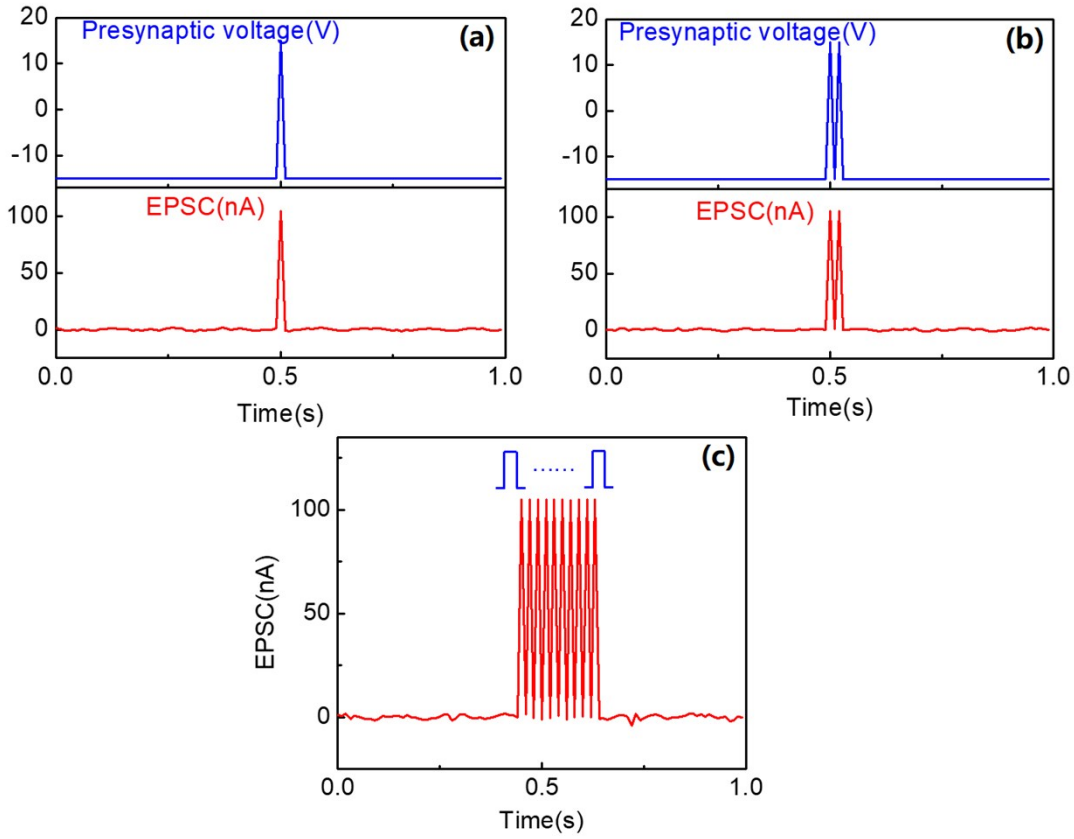

Fig. S11 (a) EPSC response for the back-gated MoS_2 FET before chitosan coating. (b) PPF behavior. (c) EPSC responses to a pulse train where the pulse width and number are respectively fixed to 10 ms and 10.

Take the original back-gated MoS_2 FET for an example, we also did a series of bionic performance tests including EPSC, PPF and dynamic filter, as shown in Fig. S11 above. We can find that after removing the gate bias all EPSC responses immediately decrease to initial values and cannot exhibit ion relaxation phenomenon like Figure 2b, 2c and 2d in our main manuscript. Current superposition effect also cannot occur even if the pulse interval is only 10 ms, as shown in Figure S11b and S11c above. Therefore, we conclude that the back-gated MoS_2 FET with the charge trapping mechanism is not a good choice to emulate the biological synapses. Of course, our presented MoS_2 synaptic device here is a proof-of-principle study on hardware implementation of artificial synapses, but our results could be a promising building block toward designing the next-generation brain-like neuromorphic computing systems to break the conventional von Neumann bottleneck.[8]

Notes and references

1 S. Woranuch and R. Yoksan, *Carbohyd. Polym.*, 2013, **96**, 495-502.

2 D. L. Zhao, X. X. Wang, X. W. Zeng, Q. S. Xia and J. T. Tang, *J. Alloy. Compd.*, 2009, **477**, 739-743.

3 S. Das, H. Y. Chen, A. V. Penumatcha and J. Appenzeller, *Nano Lett.*, 2012, **13**, 100-105.

4 K. Vanheusden, W. L. Warren, R. A. B. Devine, D. M. Fleetwood, J. R. Schwank, M. R. Shaneyfelt and Z. J. Lemnios, Nature, 1997, 386, 587.

5 R. A. B. Devine, Appl. Phys. Lett., 2000, 77, 1849-1851.

6 C. Zhong, Y. Deng, A. F. Roudsari, A. Kapetanovic, M. P. Anantram and M. Rolandi, *Nat. Commun.*, 2011, **2**, 476.

7 O. Larsson, E. Said, M. Berggren and X. Crispin, *Adv. Funct. Mater.*, 2009, **19**, 3334-3341.

8 R. Yang, K. Terabe, Y. Yao, T. Tsuruoka, T. Hasegawa, J. K. Gimzewski, and M. Aono, Nanotechnology, 2013, **24**, 384003.